Energy & Environmental Science

COMMUNICATION

View Article Online
View Journal | View Issue

Cite this: *Energy Environ. Sci.*, 2018, **11**, 1723

Received 4th April 2018,
Accepted 8th May 2018

DOI: 10.1039/c8ee00977e

rsc.li/ees

A porphyrin covalent organic framework cathode for flexible Zn–air batteries†

Bo-Quan Li, ‡ Shu-Yuan Zhang, ‡ Bin Wang, Zi-Jing Xia, Cheng Tang and Qiang Zhang *

Flexible and aqueous Zn–air batteries constitute promising next-generation energy storage devices to meet the growing demand for a safe and stable energy supply for flexible displays, wearable electronics, and implantable medical devices. However, their practical applications are severely hindered by the sluggish kinetics of the oxygen reduction reaction (ORR) and the oxygen evolution reaction (OER) at the air cathode. Herein, a porphyrin covalent organic framework (POF) was innovatively designed and applied as a cathode electrocatalyst for flexible Zn–air batteries. Porphyrin active sites were periodically constructed into well-defined two-dimensional (2D) frameworks precisely controlled at the atomic level, and carbon nanotubes (CNTs) served as scaffolds for further morphology regulation. Interwoven into a free-standing, robust, and flexible film, the as-fabricated CNT@POF hybrid demonstrates impressive performance in rechargeable liquid and flexible all-solid-state Zn–air batteries. Specifically, the liquid Zn–air battery with the CNT@POF cathode exhibits a small voltage gap of 0.71 V and outstanding stability for 200 cycles, even better than the noble-metal-based cathode. Flexible all-solid-state Zn–air batteries demonstrate a high energy efficiency of 61.6% at 1.0 mA cm^{-2} and the flexibility to stably light a red light-emitting diode (LED, 2.0 V) when bent to different degrees. This contribution demonstrates versatile and ingenious strategies for the multiscale regulation of advanced materials for energy electrocatalysis and thereby facilitates their applications in flexible and safe energy storage and conversion.

Broader context

The development of modern society stimulates the adjustment of energy infrastructure. A diversified energy supply is urgently required to meet growing energy demand on multiple occasions. Flexible and aqueous Zn–air batteries constitute an outstanding candidate for the energy supply for flexible displays, wearable electronics, and implantable medical devices, with merits in terms of intrinsic safety, high energy density, low cost, and environmental benignity. However, the cathode redox reactions are kinetically sluggish and severely limit the energy efficiency of Zn–air batteries. Therefore, the rational design of highly reactive electrocatalysts and the precise construction of flexible and stable cathodes are indispensable for working Zn–air batteries. In this contribution, a porphyrin covalent organic framework (POF) cathode was fabricated under multiscale regulation for high-performance flexible Zn–air batteries. The success of POF adds to sustainable energy storage and conversion techniques as a flexible and safe energy supply for modern life.

Introduction

Flexible and aqueous batteries constitute promising next-generation energy storage devices to meet the growing demand of safe and stable energy supplies for flexible displays, wearable electronics, and implantable medical devices.[1–4] Zn–air batteries with ultrahigh energy density (1086 W h kg^{-1}, including oxygen), an inherent aqueous electrolyte, and flexible electrodes are strongly considered to satisfy the above requirements.[5] Moreover, the atmospheric oxygen and zinc redox system endows Zn–air batteries with the advantages of natural abundance, nontoxicity, low cost, and environmental benignity. Therefore, Zn–air batteries have attracted extensive attention worldwide.[6]

A routine Zn–air battery is composed of a zinc anode, an air cathode, and an aqueous alkaline electrolyte.[7] Redox reactions of the air cathode include the oxygen reduction reaction (ORR) and the oxygen evolution reaction (OER).[8–10] Both the ORR and the OER are sluggish in kinetics with high overpotentials.[11] Poor reactivity of the air cathode results in large voltage gaps during charge and discharge, reduced energy efficiency, and inferior cycling performance, and is recognized as the bottleneck of practical applications of rechargeable Zn–air batteries.[12] Therefore, developing bifunctional ORR/OER electrocatalysts with excellent reactivity and durability is of great significance to high-performance Zn–air batteries.

Noble metal-based electrocatalysts exhibit desirable reactivity for oxygen electrocatalysts.[13,14] Pt/C and Ir/C serve as the state-of-the-art

Beijing Key Laboratory of Green Chemical Reaction Engineering and Technology, Department of Chemical Engineering, Tsinghua University, Beijing 100084, China. E-mail: zhang-qiang@mails.tsinghua.edu.cn

† Electronic supplementary information (ESI) available. See DOI: 10.1039/c8ee00977e

‡ These authors contributed equally to this work.

electrocatalysts for the ORR and the OER, respectively.[15,16] However, their scarcity, high cost, and poor durability strongly impede their large-scale application in Zn–air batteries.[17–19] On the other hand, noble-metal-free electrocatalysts have been extensively investigated as substitutes. Heteroatom-doped nanocarbon,[20] metal hydroxides,[21] oxides,[22] sulfides,[23] nitrides,[24] metal–organic frameworks,[25] and their hybrids[26–29] demonstrate considerable bifunctional performance. Nevertheless, developing bifunctional oxygen electrocatalysts remains a trial and error exploration. Insights into the rational design of bifunctional oxygen electrocatalysts and the construction of air cathodes are highly desired.

Porphyrin is a polar, conjugated, and highly-delocalized organic molecule with a strong ability to coordinate metal cations into complexes. These characteristics make porphyrin and porphyrin derived structures promising candidates for bifunctional oxygen electrocatalysis.[30,31] For instance, Sun *et al.* reported Ni^{2+} and Co^{2+} coordinated porphyrin multilayers hybridized with reduced graphene oxide sheets with an improved oxygen electrocatalytic performance.[32] Lei *et al.* noncovalently immobilized a Co^{2+} coordinated porphyrin-like complex with multiwalled carbon nanotubes for the ORR in acid solution and the OER in neutral solution.[33] Unfortunately, porphyrin small molecules exhibit low affinity with conductive scaffolds and tend to aggregate with each other, rendering reduced exposure to feedstocks. Therefore, ingenious chemical regulation and the precise control of porphyrin based electrocatalysts are required to achieve bifunctional electrocatalysts with superior reactivity and stability in Zn–air battery applications.

Considering the chemical behaviors of porphyrin small molecules, linking porphyrin units with covalent bonds into covalent organic frameworks (COFs) constitutes a reasonable strategy.[34,35] COFs represent a new family of advanced materials with periodic skeletons constructed through strong covalent interactions.[36] Directed by reticular chemistry, pre-designed functional moieties can be precisely integrated at the atomic level.[37–39] Yaghi and coworkers reported the first example of COF in 2005,[40] and COFs have demonstrated various applications in gas separation,[41] energy storage,[42] catalysis,[43] and electronics.[44] Yet, there has been no investigation of COFs as cathode materials for oxygen electrocatalysis in Zn–air batteries.

In this contribution, a porphyrin covalent organic framework (POF) was designed and applied as a cathode electrocatalyst for flexible Zn–air batteries. To fully exploit the activity of the porphyrin active sites, the POF was morphologically regulated into a thin layer (*ca.* 4 nm) uniformly coated onto a conductive long carbon nanotube (CNT) scaffold. Interwoven into a free-standing, robust, and flexible film, the as-fabricated CNT@POF hybrid demonstrates impressive performance in rechargeable liquid and flexible all-solid-state Zn–air batteries. Routine liquid Zn–air batteries with CNT@POF cathodes exhibit a low initial voltage gap of 0.71 V at 2.0 mA cm^{-2}, a high power density of 237 mW cm^{-2}, and excellent durability over 200 cycles, even better than noble-metal-based cathodes. Flexible all-solid-state Zn–air batteries with CNT@POF cathodes demonstrate a high open-circuit voltage of 1.39 V, a high energy efficiency of 61.6% at 1.0 mA cm^{-2}, and outstanding flexibility to stably light a red light-emitting diode (LED, 2.0 V) when bent to different degrees.

Results and discussion

As shown in Fig. 1a, the POF is constructed by covalently integrating porphyrin units with benzene linkages into two-dimensional (2D) layers and cobalt ions are coordinated within the porphyrin units because cobalt coordinated porphyrin has been demonstrated to be effective in many previous reports.[45,46] Further hybridization of the POF with conductive carbon nanotubes (CNTs) affords a free-standing film with flexibility introduced, which was directly employed as the cathode for Zn–air batteries. All-solid-state Zn–air batteries were assembled with the POF cathode and demonstrate desirable flexibility and safety as energy supplies (Fig. 1b).

The POF was one-pot synthesized following an acid-catalyzed dehydration reaction with benzene-1,4-dialdehyde (BDA) and pyrrole as the substrates and $Co(CH_3COO)_2{\cdot}4H_2O$ as the cobalt source. The pure POF exhibits a dense spherical morphology with a diameter of *ca.* 2.0 μm (Fig. S1, ESI†). The dense morphology with few exposed active sites suggests the pure POF alone is not suitable as an air cathode.[47] CNTs, on the other hand, serve as desirable conductive scaffolds in many electrodes.[27,48,49] In addition, the ultrahigh aspect ratio, satisfactory mechanical strength, and chemical stability of CNTs make it easy to fabricate CNT based hybrids as free-standing flexible films with high durability. Therefore, CNTs were employed as the template for POF hybridization to regulate the morphology of the POF, improve the overall conductivity, and afford a free-standing film modified with the POF.

The aligned CNTs were synthesized by an improved floating catalyst method.[50] The as-obtained CNTs exhibit a long length of 1000–2000 μm and high crystallinity (Fig. S2, ESI†). The interlayer spacing of the CNTs is 0.34 nm. Hybrids of the POF and CNTs (named CNT@POF) were fabricated by mixing pre-dispersed CNTs with POF precursors, and a free-standing CNT@POF film was fabricated by simple filtration.

Fourier-transform infrared spectrometry (FTIR) was firstly performed to evaluate the completeness of the POF synthesis. The characteristic adsorption peak of the carboxyl group of the

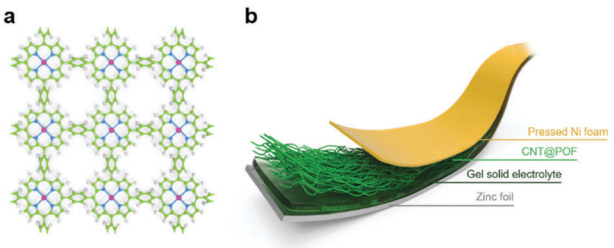

Fig. 1 Schematic of a flexible all-solid-state Zn–air battery assembled with the CNT@POF cathode. (a) Chemical structure of the single-layer POF. The hydrogen, carbon, nitrogen, and cobalt atoms are marked with white, green, blue, and pink, respectively. (b) Schematic of a flexible all-solid-state Zn–air battery.

BDA precursor at 1700 cm^{-1} is absent in CNT@POF, demonstrating the conversion of the POF precursors into desirable porphyrin structures (Fig. S3, ESI†).

The macroscopic CNT@POF film exhibits a diameter of 4.0 cm and a thickness of 250 μm (Fig. 2a and Fig. S4a, ESI†). The CNT@POF film is flexible, without any damage or cracking under bending. The CNT@POF interweave with each other to form a free-standing film (Fig. 2b). No homogeneous byproduct of POF spheres is observed, indicating the conjugated POF tends to grow on the similarly conjugated surface of the CNTs through strong intermolecular π–π interactions, affording POF uniformly coated on the CNT scaffolds (Fig. S4b, ESI†). As illustrated in the transmission electron microscope (TEM) image of CNT@POF, smooth POF layers coaxially wrap the surface of the CNTs (Fig. S5, ESI†). The thickness of the POF is measured to be *ca.* 4 nm (Fig. 2c and inset). Thin layers of POF guarantee high conductivity of the hybrid CNT@POF. Additionally, a typical 0.34 nm fringe spacing is observed, which is assigned as the (002) lattice plane of graphitized CNTs.[51] Energy dispersive spectroscopy (EDS) elemental mapping of CNT@POF exhibits a uniform distribution of carbon, nitrogen, and cobalt without aggregation (Fig. 4d). The fine elemental mapping results from the well-designed hybrid of CNT coated POF.

The structure of CNT@POF is elucidated using X-ray diffraction (XRD) techniques. The XRD patterns of CNT@POF and the CNTs reveal an intensive diffraction peak at 26° in correspondence with the (002) lattice face of the CNTs (Fig. 3a). CNT@POF, however, exhibits another prominent diffraction peak at 13°, which is the characteristic signal of the POF with intrinsic ordered structure different from amorphous polymers. As illustrated in the inset of Fig. 3a, POF layers encapsulate the CNTs coaxially. The CNT@POF hybrids are interlinked with each other and interweave into a film.

X-ray photoelectron spectroscopy (XPS) measurements were conducted to identify the elemental composition of CNT@POF. CNT@POF demonstrates a reasonable nitrogen content of 6.5 at% and a detectable cobalt content of 0.38 at% according to the XPS survey spectrum (Fig. 3b). In contrast, the nitrogen content of the CNTs is negligible (0.30 at%) and no cobalt signal was recorded. The cobalt content was further confirmed using inductively coupled plasma (ICP) optical emission spectroscopy. CNT@POF exhibits a definite cobalt content of 388.6 μg g^{-1}, while the CNTs contain no cobalt content at all (Table S1, ESI†).

High-resolution XPS spectra were recorded to evaluate the chemical conditions of CNT@POF. The N 1s high-resolution spectrum is deconvoluted into dominant pyrrole N (76.67 at%) at 400.1 eV and Co–N (23.33 at%) at 398.5 eV, implying cobalt was successfully coordinated within the porphyrin units (Fig. 3c).[52,53] The chemical shift signals at 780.0 and 795.5 eV of the Co 2p high-resolution XPS spectrum are attributed to the Co $2p_{3/2}$ and Co $2p_{1/2}$ spin–orbit peaks, respectively (Fig. S6a, ESI†), indicating evidently that cobalt is in the 2+ oxidation state and coordinated within the porphyrin units.[35,54] In contrast, no cobalt signal was afforded by the CNTs, which cannot be further deconvoluted (Fig. S6b, ESI†). Besides, the molar ratio of cobalt-coordinated nitrogen to cobalt is about 4 : 1 according to the XPS results, matching well with the theoretical composition of cobalt coordinated porphyrin. Considering the above

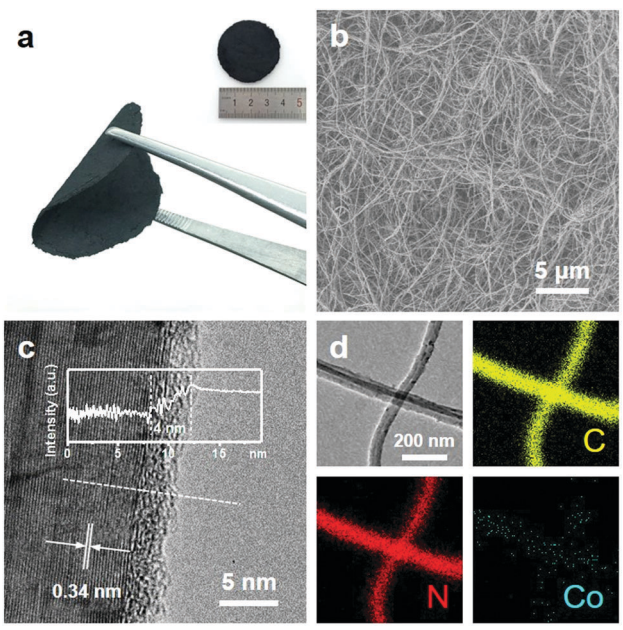

Fig. 2 Morphology characterization of CNT@POF. (a) Photograph of the free-standing CNT@POF film in the bent and extended (inset) states. (b) SEM and (c) high-resolution TEM images of CNT@POF. The inset of (c) is the contrast profile along the white dashed line. (d) TEM image and corresponding EDS elemental mapping of CNT@POF.

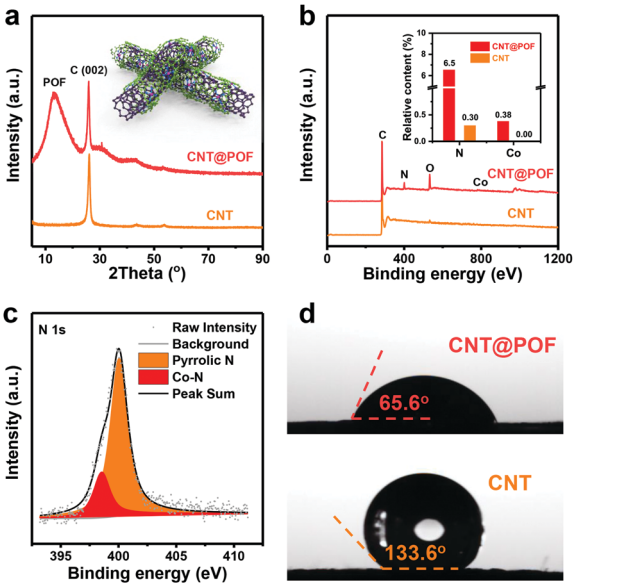

Fig. 3 Structure and composition characterization of CNT@POF. (a) XRD patterns of the CNTs and CNT@POF. The inset is the structure schematic of CNT@POF. (b) XPS survey spectra of the CNTs and CNT@POF. The inset is the corresponding relative elemental content. (c) High-resolution N 1s XPS spectrum of CNT@POF. (d) Contact angle of CNT@POF and the CNTs using the electrolyte of conventional liquid Zn–air batteries (6.0 M KOH containing 0.20 M $ZnCl_2$).

characterizations of CNT@POF, it can be comprehensively concluded that cobalt coordinated porphyrin active sites were precisely fabricated and periodically integrated to construct the pre-designed framework structure.

A superb hydrophilic surface of the air cathode ensures the easy accessibility of feedstocks to the pre-designed electrocatalytic active sites in a working Zn–air battery. Porphyrin with high polarity is a typical hydrophilic structure while CNTs with a non-polar surface are highly hydrophobic. Therefore, CNT@POF with a modified polar surface inherits the hydrophilia of the porphyrin functional units and significantly improves the disadvantages of CNTs. The hydrophilia of the CNTs and CNT@POF was evaluated by measuring the contact angles with a practical electrolyte (6.0 M KOH + 0.20 M $ZnCl_2$). The CNT@POF offers a much smaller contact angle of 65.6° than the CNTs of 133.6°, indicating a more hydrophilic surface for aqueous Zn–air batteries (Fig. 3d).

Proved by the comprehensive characterizations discussed above, POF@CNT reveals ingenious structural design to afford well-defined cobalt coordinated porphyrin active sites under precise control, a highly exposed hydrophilic surface inherited from polar porphyrin, interlinked 3D electron pathways constructed by interweaved CNTs, abundant internal ion/gas channels for bifunctional ORR/OER electrocatalysis at triple phase boundaries, and the intrinsic flexibility provided by the free-standing CNT@POF film. In addition, the mechanical rigidity attributed by the CNT scaffolds and the chemical stability of the covalently constructed POF endow CNT@POF with promising stability. Considering these unique advantages, CNT@POF inspires further applications as an emerging cathode material for flexible Zn–air batteries.

A liquid Zn–air battery was assembled to evaluate the bifunctional electrocatalytic performance of CNT@POF. A polished zinc foil was used as the anode. 6.0 M KOH aqueous solution served as the electrolyte. 0.20 M $ZnCl_2$ was added to the electrolyte to ensure reversible Zn redox reactions at the anode.[55] A CNT@POF film was hot-pressed with a hydrophobic gas diffusion layer (GDL) before being used as the cathode to construct a suitable triple phase boundary for oxygen redox reactions. The areal loading of the POF is 1.50 mg cm^{-2}. Cathodes with state-of-the-art noble metal electrocatalysts were fabricated as a comparison. Pt/C for the ORR and Ir/C for the OER were mixed with a mass ratio of 1 : 1. The areal loading of the noble metal electrocatalysts is identical to that of the POF, and the cathode is named Pt/C + Ir/C. In addition, POF spheres were mechanically mixed with CNT scaffolds to afford another control cathode named CNT + POF to demonstrate the advantages of the hybrid structure of CNT@POF.

The electrocatalytic performance was firstly evaluated by polarization curves (Fig. 4a). The Zn–air battery with the CNT@POF cathode delivers higher current density over the Pt/C + Ir/C cathode. The discharge and charge potentials required for a current density of 20.0 mA cm^{-2} are 1.21 and 1.99 V for CNT@POF, respectively. In contrast, the Pt/C + Ir/C cathode requires a discharge potential of 0.95 V and a charge potential of 2.02 V to deliver the same current density. The reduced overpotentials strongly indicate the superior

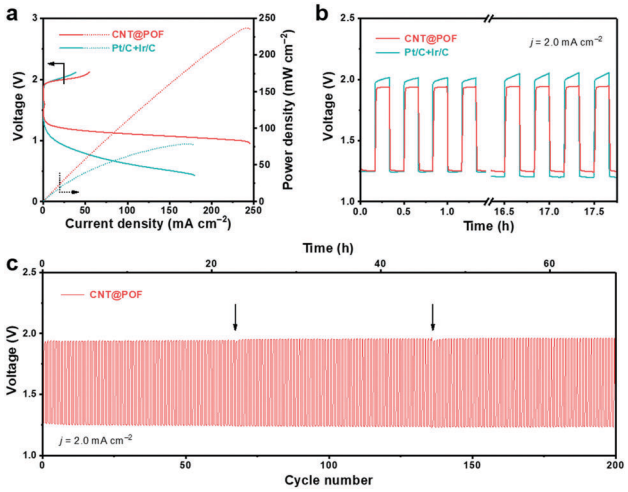

Fig. 4 Electrochemical evaluation of CNT@POF in rechargeable liquid Zn–air batteries. (a) Polarization curves and (b) galvanostatic discharge–charge cycling curves at 2.0 mA cm^{-2} of CNT@POF and Pt/C + Ir/C. (c) Long time cycling test of CNT@POF at 2.0 mA cm^{-2} (arrows represent replacing the old electrolyte).

electrochemical reactivity of CNT@POF over Pt/C + Ir/C. Consequently, the CNT@POF cathode affords an impressive peak power density of 237 mW cm^{-2}, evidently outperforming the reference Pt/C + Ir/C cathode (78 mW cm^{-2}) and the majority of recently reported bifunctional electrocatalysts applied in rechargeable liquid Zn–air batteries (Table S2, ESI†). On the other hand, the CNT + POF cathode delivers larger voltage windows at 20.0 mA cm^{-2} (0.90 V for discharge and 2.12 V for charge) and a lower peak power density of 57 mW cm^{-2}, suggesting the hybrid structure of CNT@POF improves the bifunctional reactivity by fully exposing the POF active sites through morphology regulation (Fig. S7, ESI†).

Galvanostatical discharge tests were conducted at a current density of 20.0 mA cm^{-2} to determine the specific capacity of the Zn–air batteries (Fig. S8, ESI†). Normalized to the mass of consumed zinc, the specific capacity was calculated to be 772.7 mA h g^{-1} for CNT@POF, higher than that of Pt/C + Ir/C (738.6 mA h g^{-1}).

The cycling performance is of great significance to practical applications of rechargeable Zn–air batteries. Fig. 4b presents the galvanostatical discharge–charge cycling curves at 2.0 mA cm^{-2}. The initial discharge voltages are both 1.25 V for the CNT@POF cathode and the Pt/C + Ir/C cathode. However, the initial charge voltage is 1.96 V for the CNT@POF cathode and 2.02 V for the Pt/C + Ir/C cathode, respectively. Benefitting from the lower charge voltage, the charge/discharge voltage gap of CNT@POF is 0.71 V, which is smaller than that of Pt/C + Ir/C (0.77 V). The smaller voltage gap of CNT@POF suggests higher bifunctional ORR/OER reactivity than Pt/C + Ir/C and is in agreement with the polarization curves. Consequently, the energy efficiency is 63.8% with the CNT@POF cathode and 61.9% with the Pt/C + Ir/C cathode, respectively. The CNT + POF cathode, however, affords a minimum voltage gap of 0.83 V and a reduced energy efficiency of 58.5% (Fig. S9, ESI†). The inferior

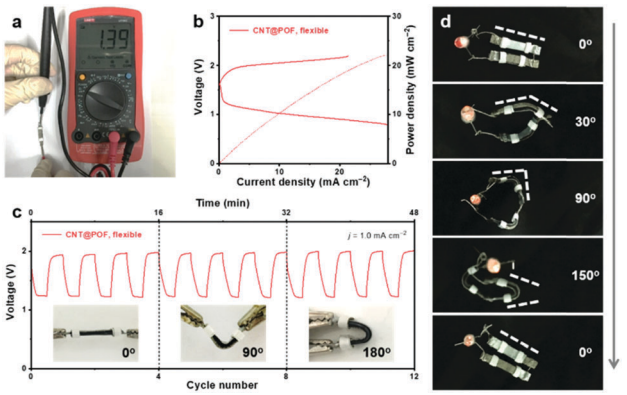

Fig. 5 Application of CNT@POF in rechargeable flexible all-solid-state Zn–air batteries. (a) Open-circuit voltage and (b) polarization curves of the flexible all-solid-state Zn–air battery with the CNT@POF cathode. (c) Galvanostatic discharge–charge cycling curves at 1.0 mA cm^{-2} under bending at 0°, 90°, and 180°, respectively. (d) Photographs of a commercial red LED lit by two flexible all-solid-state Zn–air batteries connected in series when bent to various angles.

performance of the CNT + POF cathode is attributed to the adverse morphology and weak interaction between the POF and the CNTs. After cycling for over 17 h, the Zn–air battery with the CNT@POF cathode exhibits a constant charge/discharge voltage gap of 0.71 V. In contrast, the charge/discharge voltage gap increases to 0.79 V in the case of Pt/C + Ir/C.

To further investigate the long-term cycling stability of the cathode materials, galvanostatical discharge–charge cycling tests were performed at 2.0 mA cm^{-2} for 200 cycles (Fig. 4c). The CNT@POF cathode exhibits extraordinary stability without an obvious voltage gap change, while the Pt/C + Ir/C cathode and the CNT + POF cathode severely suffer from activity decay. The voltage gap of the Pt/C + Ir/C cathode increased to 0.98 V after 200 cycles (Fig. S10, ESI†), and a 100 mV increase was observed in the voltage gap for the CNT + POF cathode (Fig. S9, ESI†). At a relatively high current density of 25.0 mA cm^{-2}, the Zn–air battery with the CNT@POF cathode is still stable with the charge/discharge voltage gap maintained at 1.00 V for 12 cycles (Fig. S11, ESI†). Therefore, CNT@POF demonstrates higher stability over Pt/C + Ir/C and CNT + POF as the cathode material under the working conditions of rechargeable liquid Zn–air batteries.

The superb performance of the rechargeable liquid Zn–air battery and the intrinsic mechanical flexibility support CNT@POF as the cathode material for flexible all-solid-state Zn–air batteries. The CNT@POF film served directly as the air cathode with a flexible Zn foil as the anode, alkaline polyvinyl alcohol gel as the electrolyte, and pressed Ni foam as the current collectors, to construct a flexible all-solid-state Zn–air battery (as illustrated in Fig. 1b). The flexible all-solid-state Zn–air battery exhibits a high open-circuit voltage of 1.39 V (Fig. 5a). The discharge and charge polarization curves of the flexible all-solid-state Zn–air battery illustrate a small voltage gap identical to that of the liquid Zn–air battery, indicating comparable electrocatalytic performance under varied conditions (Fig. 5b). The maximum peak power density is measured to be as high as 22.3 mW cm^{-2}. The as-fabricated flexible all-solid-state Zn–air battery exhibits stable discharge and charge voltages of 1.22 and 1.98 V, respectively, at 1.0 mA cm^{-2} when bent to different angles (Fig. 5c), appearing to be a promising flexible and safe energy conversion system with a high energy efficiency of 61.6% achieved simultaneously. To further investigate the practical application, two flexible all-solid-state Zn–air batteries were connected in series to light a commercial red light-emitting diode (LED, 2.0 V). When the batteries were bent to 0°, 30°, 90°, and 150° in sequence and finally returned to 0°, the red LED was stably and continuously lit (Fig. 5d). The demonstration of flexible all-solid-state Zn–air batteries shows their potential applications for wearable electronics.

Flexible all-solid-state batteries have been occupying a growing proportion of the energy source configuration of modern society in the bigger picture. Zn–air batteries with facile flexibility and inherent safety are recognized as a prominent candidate to fulfill next-generation energy demands. The innovation of electrode materials is a direct driving force for advanced energy storage. COFs as a new family of advanced materials were herein extended to flexible all-solid-state Zn–air batteries for the first time and offer the advantages of (1) well-defined active sites that can be pre-designed, (2) strong covalent linkages to integrate the active sites, (3) versatility in composition, morphology regulation and material composition, and (4) potential for pre- or post-synthetic modification. The CNT@POF herein demonstrates a potent example for COFs and other material families to be explored in energy related techniques.

Conclusions

A porphyrin covalent organic framework cathode was rationally designed and fabricated for flexible Zn–air batteries. The cobalt coordinated porphyrin units were covalently linked into 2D frameworks under precise chemical control at the atomic level. The POF layers were facilely coated on the surface of conductive carbon nanotubes as hybrids for morphology and interfacial regulation at the nanoscale. The resultant CNT@POF interweaved into a macroscopic free-standing flexible film and served as an excellent cathode material for bifunctional oxygen electrocatalysis in Zn–air batteries. Rechargeable liquid Zn–air batteries with the CNT@POF cathode exhibit satisfactory performance superior to noble metal electrocatalysts with a low initial voltage gap of 0.71 V, a high power density of 237 mW cm^{-2}, and durability over 200 cycles. Further application of the CNT@POF cathode in a flexible all-solid-state Zn–air battery reveals promising potential as a flexible and safe energy supply for wearable devices and electronics. This contribution demonstrates versatile and ingenious strategies for the multiscale regulation of advanced materials for energy electrocatalysis and thereby facilitates their applications in flexible and safe energy storage and conversion.

Conflicts of interest

There are no conflicts to declare.

Acknowledgements

This work was supported by National Key Research and Development Program (2016YFA0202500, 2015CB932500, and 2016YFA0200102), National Natural Scientific Foundation of China (21676160), and Tsinghua University Initiative Scientific Research Program. We thank Hao-Fan Wang, Chen-Yu Chen, Chang-Xin Zhao, and Dr Xiaoyang Cui for helpful discussion.

Notes and references

1 X. Wang, X. Lu, B. Liu, D. Chen, Y. Tong and G. Shen, *Adv. Mater.*, 2014, **26**, 4763–4782.
2 H. J. Peng, J. Q. Huang and Q. Zhang, *Chem. Soc. Rev.*, 2017, **46**, 5237–5288.
3 Y. Lu, J. B. Goodenough and Y. Kim, *J. Am. Chem. Soc.*, 2011, **133**, 5756–5759.
4 T. Janoschka, N. Martin, U. Martin, C. Friebe, S. Morgenstern, H. Hiller, M. D. Hager and U. S. Schubert, *Nature*, 2015, **527**, 78–81.
5 L. Li, Z. Wu, S. Yuan and X.-B. Zhang, *Energy Environ. Sci.*, 2014, **7**, 2101–2122.
6 Y. Li and H. Dai, *Chem. Soc. Rev.*, 2014, **43**, 5257–5275.
7 J. Fu, Z. P. Cano, M. G. Park, A. Yu, M. Fowler and Z. Chen, *Adv. Mater.*, 2017, **29**, 1700610.
8 D. U. Lee, J.-Y. Choi, K. Feng, H. W. Park and Z. Chen, *Adv. Energy Mater.*, 2014, **4**, 1301389.
9 V. Neburchilov, H. Wang, J. J. Martin and W. Qu, *J. Power Sources*, 2010, **195**, 1271–1291.
10 Y. P. Zhu, C. Guo, Y. Zheng and S. Z. Qiao, *Acc. Chem. Res.*, 2017, **50**, 915–923.
11 Y. Jiao, Y. Zheng, M. Jaroniec and S. Z. Qiao, *Chem. Soc. Rev.*, 2015, **44**, 2060–2086.
12 F. Cheng and J. Chen, *Chem. Soc. Rev.*, 2012, **41**, 2172–2192.
13 C. C. McCrory, S. Jung, J. C. Peters and T. F. Jaramillo, *J. Am. Chem. Soc.*, 2013, **135**, 16977–16987.
14 N. Zhang, Y. Feng, X. Zhu, S. Guo, J. Guo and X. Huang, *Adv. Mater.*, 2017, **29**, 1603774.
15 J. Li, A. Alsudairi, Z. F. Ma, S. Mukerjee and Q. Jia, *J. Am. Chem. Soc.*, 2017, **139**, 1384–1387.
16 T. Reier, M. Oezaslan and P. Strasser, *ACS Catal.*, 2012, **2**, 1765–1772.
17 B. Q. Li, S. Y. Zhang, C. Tang, X. Cui and Q. Zhang, *Small*, 2017, **13**, 1700610.
18 Y. Wang, Y. Zhang, Z. Liu, C. Xie, S. Feng, D. Liu, M. Shao and S. Wang, *Angew. Chem., Int. Ed.*, 2017, **56**, 5867–5871.
19 L. Trotochaud, S. L. Young, J. K. Ranney and S. W. Boettcher, *J. Am. Chem. Soc.*, 2014, **136**, 6744–6753.
20 C. Tang and Q. Zhang, *Adv. Mater.*, 2017, **29**, 1604103.
21 L. Qian, Z. Lu, T. Xu, X. Wu, Y. Tian, Y. Li, Z. Huo, X. Sun and X. Duan, *Adv. Energy Mater.*, 2015, **5**, 1500245.
22 H.-F. Wang, C. Tang, X. Zhu and Q. Zhang, *J. Mater. Chem. A*, 2016, **4**, 3379–3385.
23 Q. Liu, J. Jin and J. Zhang, *ACS Appl. Mater. Interfaces*, 2013, **5**, 5002–5008.
24 F. Meng, H. Zhong, D. Bao, J. Yan and X. Zhang, *J. Am. Chem. Soc.*, 2016, **138**, 10226–10231.
25 H. Wang, F. Yin, G. Li, B. Chen and Z. Wang, *Int. J. Hydrogen Energy*, 2014, **39**, 16179–16186.
26 Y. Li, M. Gong, Y. Liang, J. Feng, J. E. Kim, H. Wang, G. Hong, B. Zhang and H. Dai, *Nat. Commun.*, 2013, **4**, 1805.
27 X. Han, X. Wu, C. Zhong, Y. Deng, N. Zhao and W. Hu, *Nano Energy*, 2017, **31**, 541–550.
28 C. Tang, L. Zhong, B. Zhang, H. F. Wang and Q. Zhang, *Adv. Mater.*, 2018, **30**, 1705110.
29 J. Yin, Y. Li, F. Lv, Q. Fan, Y. Q. Zhao, Q. Zhang, W. Wang, F. Cheng, P. Xi and S. Guo, *ACS Nano*, 2017, **11**, 2275–2283.
30 A. Zitolo, V. Goellner, V. Armel, M. T. Sougrati, T. Mineva, L. Stievano, E. Fonda and F. Jaouen, *Nat. Mater.*, 2015, **14**, 937–942.
31 Z. Sun, J. Li, H. Zheng, X. Liu, S. Ye and P. Du, *Int. J. Hydrogen Energy*, 2015, **40**, 6538–6545.
32 T. Zhang, N. Imanishi, Y. Takeda and O. Yamamoto, *Chem. Lett.*, 2011, **40**, 668–673.
33 H. Lei, C. Liu, Z. Wang, Z. Zhang, M. Zhang, X. Chang, W. Zhang and R. Cao, *ACS Catal.*, 2016, **6**, 6429–6437.
34 C. Y. Lin, L. Zhang, Z. Zhao and Z. Xia, *Adv. Mater.*, 2017, **29**, 1606635.
35 Z. S. Wu, L. Chen, J. Liu, K. Parvez, H. Liang, J. Shu, H. Sachdev, R. Graf, X. Feng and K. Mullen, *Adv. Mater.*, 2014, **26**, 1450–1455.
36 C. S. Diercks and O. M. Yaghi, *Science*, 2017, **355**, 923–931.
37 N. Huang, P. Wang and D. Jiang, *Nat. Rev. Mater.*, 2016, **1**, 16068.
38 O. M. Yaghi, M. O'Keeffe, N. W. Ockwig, H. K. Chae, M. Eddaoudi and J. Kim, *Nature*, 2003, **423**, 705–714.
39 F.-Y. Yi, R. Zhang, H. Wang, L.-F. Chen, L. Han, H.-L. Jiang and Q. Xu, *Small Methods*, 2017, **1**, 1700187.
40 A. P. Cote, A. I. Benin, N. W. Ockwig, M. O'Keeffe, A. J. Matzger and O. M. Yaghi, *Science*, 2005, **310**, 1166–1170.
41 S. Zhao, B. Dong, R. Ge, C. Wang, X. Song, W. Ma, Y. Wang, C. Hao, X. Guo and Y. Gao, *RSC Adv.*, 2016, **6**, 38774–38781.
42 J. Zhou and B. Wang, *Chem. Soc. Rev.*, 2017, **46**, 6927–6945.
43 S. Y. Ding, J. Gao, Q. Wang, Y. Zhang, W. G. Song, C. Y. Su and W. Wang, *J. Am. Chem. Soc.*, 2011, **133**, 19816–19822.
44 C. R. DeBlase, K. E. Silberstein, T. T. Truong, H. D. Abruna and W. R. Dichtel, *J. Am. Chem. Soc.*, 2013, **135**, 16821–16824.
45 A. D. Alder, F. R. Longo and W. Shergalis, *J. Am. Chem. Soc.*, 1964, **86**, 3145.
46 H. A. O. Hill, A. J. Macfarlane and R. J. P. Williams, *J. Chem. Soc. A*, 1969, 1704–1707.
47 B. Nath, W.-H. Li, J.-H. Huang, G.-E. Wang, Z.-h. Fu, M.-S. Yao and G. Xu, *CrystEngComm*, 2016, **18**, 4259–4263.
48 Z. Yuan, H.-J. Peng, J.-Q. Huang, X.-Y. Liu, D.-W. Wang, X.-B. Cheng and Q. Zhang, *Adv. Funct. Mater.*, 2014, **24**, 6105–6112.
49 C. Ma, N. Xu, J. Qiao, S. Jian and J. Zhang, *Int. J. Hydrogen Energy*, 2016, **41**, 9211–9218.

50 Q. Zhang, D.-G. Wang, J.-Q. Huang, W.-P. Zhou, G.-H. Luo, W.-Z. Qian and F. Wei, *Carbon*, 2010, **48**, 2855–2861.
51 S. Thieme, J. Brückner, I. Bauer, M. Oschatz, L. Borchardt, H. Althues and S. Kaskel, *J. Mater. Chem. A*, 2013, **1**, 9225–9234.
52 Y. Qian, Z. Liu, H. Zhang, P. Wu and C. Cai, *ACS Appl. Mater. Interfaces*, 2016, **8**, 32875–32886.
53 P. Yin, T. Yao, Y. Wu, L. Zheng, Y. Lin, W. Liu, H. Ju, J. Zhu, X. Hong, Z. Deng, G. Zhou, S. Wei and Y. Li, *Angew. Chem., Int. Ed.*, 2016, **55**, 10800–10805.
54 A. N. Oldacre, A. E. Friedman and T. R. Cook, *J. Am. Chem. Soc.*, 2017, **139**, 1424–1427.
55 C. Zhang, N. Mahmood, H. Yin, F. Liu and Y. Hou, *Adv. Mater.*, 2013, **25**, 4932–4937.